




Visible-light optical limiting of vanadia–polyvinylpyrrolidone nanofibers

Yasemin Pepe¹, Yusuf Tutel⁴, Serife Akkoyun^{2,3,*}, Nurcan Ascı², Eda Cevik⁴, Ahmet Karatay^{1,*} , Husnu Emrah Unalan^{4,5,*}, and Ayhan Elmali¹

¹ Department of Engineering Physics, Faculty of Engineering, Ankara University, 06100 Ankara, Turkey

² Department of Metallurgical and Materials Engineering, Faculty of Engineering and Natural Sciences, Ankara Yıldırım Beyazıt University, 06010 Ankara, Türkiye

³ Central Research Laboratory, Application and Research Center, Ankara Yıldırım Beyazıt University, 06010 Ankara, Turkey

⁴ Department of Metallurgical and Materials Engineering, Middle East Technical University (METU), 06800 Ankara, Turkey

⁵ Energy Storage Materials and Devices Research Center (ENDAM), Middle East Technical University (METU), 06800 Ankara, Turkey

Received: 19 October 2023

Accepted: 12 February 2024

Published online:
8 March 2024

© The Author(s), 2024

ABSTRACT

In this work, vanadium pentoxide (V_2O_5) nanoparticles-filled electrospun polyvinylpyrrolidone (PVP) nanofibers were investigated systematically at various nanofiller weight percentages (8 and 10 wt%) and input intensities to reveal the effective optical limiting feature in the visible spectrum. XRD analysis demonstrated the purity of the produced V_2O_5 nanoparticles. According to SEM findings, V_2O_5 nanoparticles were effectively integrated into the PVP nanofibers. Two distinct absorption bands were observed at around 400 and 217 nm. These bands were related to PVP and V_2O_5 nanoparticles in linear absorption measurements, respectively. Moreover, an increased Urbach energy value was obtained with an increase in V_2O_5 nanofiller content within PVP. Open-aperture Z-scan measurements were taken at 532 nm considering the band gap energy of the V_2O_5 nanofillers in PVP composite nanofibers. In 8 wt% V_2O_5 nanofilled PVP nanofibers, one-photon absorption (OPA) was the main nonlinear absorption (NA) mechanism, and the defect states of the V_2O_5 nanoparticles had no contribution to NA. On the other hand, sequential two-photon absorption was the main NA mechanism, and the defect states of the nanoparticles caused more efficient NA behavior in 10 wt% V_2O_5 nanofilled PVP nanofibers. The effective optical limiting behavior was obtained for this composite nanofiber with lower limiting threshold as 1.49×10^{-5} J/cm². The V_2O_5 nanofilled PVP nanofibers presented strong potential optical limiters in the visible wavelength region. This was attributed to their high linear transmittance at low input intensities and their robust NA behavior at higher input intensities.

Handling Editor: Christopher Blanford.

Address correspondence to E-mail: serife.akkoyun@aybu.edu.tr; akaratay@eng.ankara.edu.tr; unalan@metu.edu.tr

Introduction

High-level requirements for an ideal optical limiter include broadband optical limiting capability across the whole visible spectrum as well as broadband temporal capability from the sub-nanosecond to continuous regimes [1]. The development of the perfect broadband optical limiting materials has undergone a great deal of effort. These efforts are based on a variety of phenomena, such as saturable absorption, multiphoton absorption, nonlinear scattering, and nonlinear absorption. The material with high nonlinearity has many applications, including optical switches, optical limiters, lithium batteries, smart windows, and gas sensors [2–6]. Vanadium oxides are transition metal oxides (TMOs) with oxidation states of +2 to +5. Due to high oxygen-to-vanadium (O/V) ratio, vanadium pentoxide (V_2O_5) is the most stable phase and exhibits a phase transition at 257 °C [7, 8]. It has been the most studied vanadium oxide phase, due to its unique transition behavior from semiconductor to metal, with a wide optical band gap, improved thermal and chemical stability with excellent thermoelectric features [9–11]. Nevertheless, bulk V_2O_5 faces limitations due to its low vanadium dissolution issues, electrical conductivity, and slow reaction kinetics [12, 13]. The use of V_2O_5 has been demonstrated widely in gas sensors [14, 15], catalysis [16], electrochromic [17, 18], optoelectronic applications [19, 20], and solar cells [21, 22].

Nanoparticles can be incorporated into polymeric matrices to create nanofibers, ultimately enhancing their properties and introducing novel functionalities [23]. This allows modification of their physical, chemical, electrical, or optical characteristics. For example, metal oxide nanoparticles enhance tensile strength, while metal nanoparticles facilitate electrical conductivity within the nanofiber structure. Furthermore, to add optical functionalities, nanoparticles with particular optical properties can be included into nanofibers which are suited for use in light-emitting devices, sensors, and photonics.

It has been demonstrated that two-photon absorption causes substantial optical limiting (OL) in a number of semiconductors, including ZnSe, CdS, PbS, and ZnO, as well as in various organic materials [24–29]. However, few studies exist on the OL behavior of V_2O_5 . Parida et al. examined optical limiting features of V_2O_5 nanoflowers based on three-photon absorption [30]. It was reported that the optical

limiting behavior of V_2O_5 nanoflowers resulted from an effective three-photon absorption mechanism. Poonam et al. examined the OL response of the $V_2O_5:MoO_3$ thin films [31]. Nonlinear absorption was reported to be enhanced with increasing thickness in the MoO_3 -doped sample. Saravanakannan et al. investigated the nonlinear absorption (NA) and OL behavior of the fluorine-doped V_2O_5 nanoparticles [32]. It was reported that the exhibited nonlinear absorption was due to genuine two-photon absorption process. OL response of the V_2O_5 thin films was also investigated by our group [33]. We observed defect-assisted nonlinear absorption behavior in V_2O_5 thin films and found that annealing at 450 °C enhances both the nonlinear absorption and optical limiting behavior.

In the literature, the nonlinear optical properties of the nanocomposite films have been extensively investigated [34–39] due to the combination of unique properties of nanoparticles and advantages of polymers. Beside these, there are few studies related with the nonlinear optical properties of the composite nanofibers. Pramod et al. reported the nonlinear optical character of electrospun benzil-poly(methyl methacrylate) (PMMA) nanofibers [40]. They reported that the nanofibers showed saturable absorption behavior at low input intensity and nonlinear absorption at higher input intensities. Yogeswari et al. examined the OL behavior of potassium dihydrogen phosphate (KDP)–polyethylene oxide (PEO) electrospun nanofibers [41]. They revealed that the excited-state absorption process played a dominant role in the observed nonlinearity and two-photon absorption was responsible for the observed OL performance. On the other hand, there is no study examining the linear optical features, charge transfer mechanisms, and OL features with limiting thresholds of the V_2O_5 nanoparticles-filled PVP composite nanofibers to the best of our knowledge. Nanoparticles have an exceedingly high surface-to-volume ratio owing to their small dimensions. This property increases the light–matter interactions compared to the bulk materials. Besides, nanofibers have high aspect ratio (length-to-diameter ratio), and this property supports increased light–matter interaction like in nanoparticles. The combined system (nanofibers filled with nanoparticles) should have higher light–matter interactions than either material. High light–matter interactions are possible due to the

nanofibrous structure of electrospun mats, which significantly influences the materials' nonlinear optical properties. Therefore, in this work, V_2O_5 nanoparticles synthesized by the hydrothermal method were used as nanofillers in PVP nanofibers. Wide band gap of PVP enabled the use of these composite nanofibers in a wide spectral range. Open-aperture (OA) Z-scan measurements were taken at 532 nm under diverse input intensities considering band gap energies of the composite nanofibers and their defect states created by V_2O_5 nanoparticles. Linear optical features, charge transfer mechanisms, and OL features with limiting thresholds of the PVP/ V_2O_5 composite nanofibers were reported for the first time.

Materials and methods

Materials

Ammonium metavanadate (NH_4VO_3), ethanol (CH_3CH_2OH), and nitric acid (HNO_3) (65.0%) were purchased from Sigma-Aldrich. The polymer used is a polyvinylpyrrolidone (PVP) supplied from ACROS Organics. N–N dimethylformamide (DMF—ISOLAB, purity $\geq 99.0\%$) was used as solvent.

Synthesis of V_2O_5 nanoparticles and production of V_2O_5 composite nanofibers

V_2O_5 powders were produced through hydrothermal synthesis, as reported by Mu et al. [42]. For the precursor solution, 0.819 g of NH_4VO_3 was dissolved in 70 ml of ethanol with the help of nitric acid (2–3 ml). Nitric acid was used to adjust the precursor solution's pH to about 3–4. The obtained precursor solution was vigorously stirred for half an hour. Subsequently, the solution was transferred to a Teflon-lined autoclave for reaction in an oven at 180 °C for 24 h. The obtained particles were then washed with water and ethanol several times before drying at 80 °C for 10 h. Lastly, the obtained powder was annealed at 500 °C for 1 h.

A schematic for the fabrication procedure of the nanofibers is provided in Fig. 1. A 20 wt% PVP in DMF solution was prepared with constant stirring at ambient temperature. Afterward, PVP solutions containing 8 and 10 wt% (% of PVP) of V_2O_5 nanoparticles were prepared. The nanoparticles were dispersed in polymer solutions through ultrasonication by a BANDELIN GM 2200 ultrasonic homogenizer. Then, electrospinning was performed at ambient temperature. The tip-to-collector distance of 15 cm, high voltage of 17.5 kV,

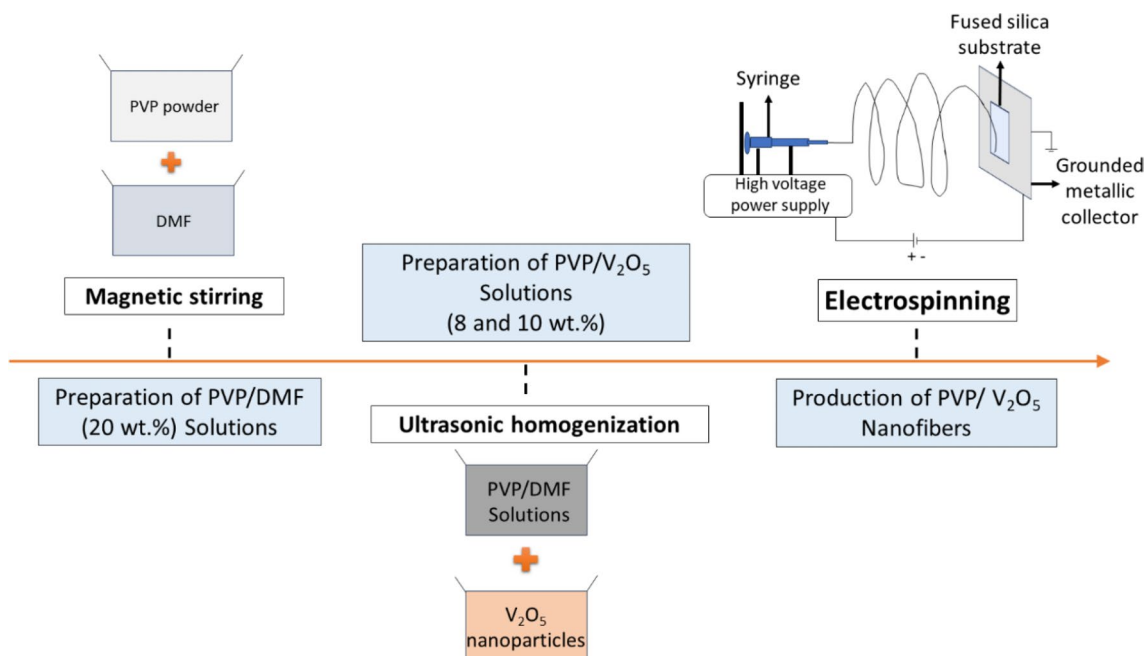


Figure 1 Schematic diagram for the production of electrospun PVP and PVP/ V_2O_5 nanofibers.

and the flow velocity of 0.25 ml/h were found to be the ideal processing parameters. The nanofibers were electrospun onto fused silica substrates to take optical measurements. The obtained composite nanofibers were labeled as PVP/V₂O₅-8 and PVP/V₂O₅-10 for 8 and 10 wt% of V₂O₅ nanoparticles-filled PVP nanofibers, respectively.

Characterizations

The crystal structure of the powders was identified by Rigaku D/Max-2000 diffractometer with Cu K radiation operating at 40 kV from 10° to 90° at a scan rate of 0.5°/min, and FEI Nova Nano FEG-SEM model scanning electron microscope (SEM) was used to examine the morphology of the powders. The surface chemistry and oxidation state of the elements in the powders were examined using X-ray photoelectron spectroscopy (XPS) and Raman spectroscopy. A monochromatic Al K_α X-ray source (15 kV, 400 W) and a SPECS PHOIBOS hemispherical analyzer were used to perform the XPS investigations. As a benchmark, the nominal binding energy (B.E.) of the C1s signal, which is 284.68 eV, was chosen. With a 532-nm Nd:YAG laser as the excitation source, Raman spectra were recorded using a BRUKER FRA 106/S spectrometer. Using a Malvern Nano ZS, photon correlation spectroscopy was used to measure the average particle size of the nanoparticles dispersed in water. SEM images and EDS maps of the nanofibers were captured with a HITACHI SU5000 field emission scanning electron microscope (SEM) equipped with an Oxford X-MaxN 80 energy-dispersive X-ray spectroscopy (EDS). All nanofibers were sputter coated with gold (Au) prior to analysis. Aluminum tape was used instead of carbon tape for SEM-EDS sample preparation to improve the contrast during analysis; 100 nanofibers were used to estimate their average diameters using ImageJ software (NIH—USA). The composite nanofibers thicknesses were measured by a spectroscopic ellipsometer (Woollam M-2000V) at three angles of incidence (65, 70, and 75°). The thicknesses of the composite nanofiber mats were found as 1.3 μm. Shimadzu UV-1800 model UV-Vis spectrophotometer was used to reveal the linear optical absorption feature-related band gaps of the composite nanofibers. To observe the possible defect states constructed emission, photoluminescence measurements were taken by PerkinElmer LS55 spectrophotometer. Q-switched Nd:YAG (Quantel Brilliant) laser (4-ns pulse duration, 10-Hz repetition

rate) at 532 nm was used to observe the nonlinear absorption (NA) behavior of the composite nanofibers with OA Z-scan measurements. The obtained results were evaluated for their optical limiting features.

Results and discussion

Morphological and structural properties of V₂O₅ nanopowders

The morphology of the V₂O₅ nanopowders was investigated by SEM analysis, and a representative micrograph is provided in Fig. 2a. The SEM image primarily showed aggregated irregular-shaped nanoparticles. All nanoparticles were dispersed in water to determine their average particle size using photon correlation spectroscopy. The *d* (0.5) and *d* (0.9) values were found to be around 235 and 432 nm, respectively. The XRD pattern of the synthesized V₂O₅ nanopowders is provided in Fig. 2b. The diffraction pattern was indexed to JCPDS #41-1426 with major diffraction peaks at 15.41°, 20.32°, 21.74°, 26.10°, 31.01°, 32.43°, 34.39°, 47.31°, and 51.23° corresponding to lattice planes of (200), (001), (101), (110), (301), (011), (310), (600), and (020), respectively. This indicated a pure orthorhombic phase of V₂O₅ [42–45]. No impurity peaks were obtained, proving the purity of the synthesized V₂O₅ nanopowders.

XPS spectra for V2*p* core levels and O1s are provided in Fig. 2c and d, respectively. According to Silversmit et al. [46], V2*p*_{3/2} signals appeared at 517.2, 515.8, 515.3, 513.7, 512.4 eV for the V⁵⁺, V⁴⁺, V³⁺, V²⁺, V⁰ states, respectively. In Fig. 2c, it is evident that apart from the major O1s signal at 529.9 eV, there are three distinct V2*p* XPS signals detected at 524.6, 517.1, and 515.7 eV. These signals can be ascribed to the V⁵⁺2*p*_{1/2}, V⁵⁺2*p*_{3/2}, and V⁴⁺2*p*_{3/2} states, respectively, in great harmony with the literature [17, 33, 46–48]. This confirmed that the predominant oxidation state of vanadium ions was +5. It is also important to highlight that the binding energy (B.E.) position between the V⁵⁺2*p*_{3/2} and O1s signals has a value of Δ = 12.8 eV. Moreover, there is a spin-orbit splitting difference of Δ = 7.5 eV between the V⁵⁺2*p*_{1/2} and V⁵⁺2*p*_{3/2} signals. These findings strongly supported the conclusion that the vanadium oxidation state of +5 is the dominant phase, consistent with previous studies [17, 46, 47]. On the other hand, the most intense signal at 529.9 eV in the O1s spectrum indicated the existence of a V–O

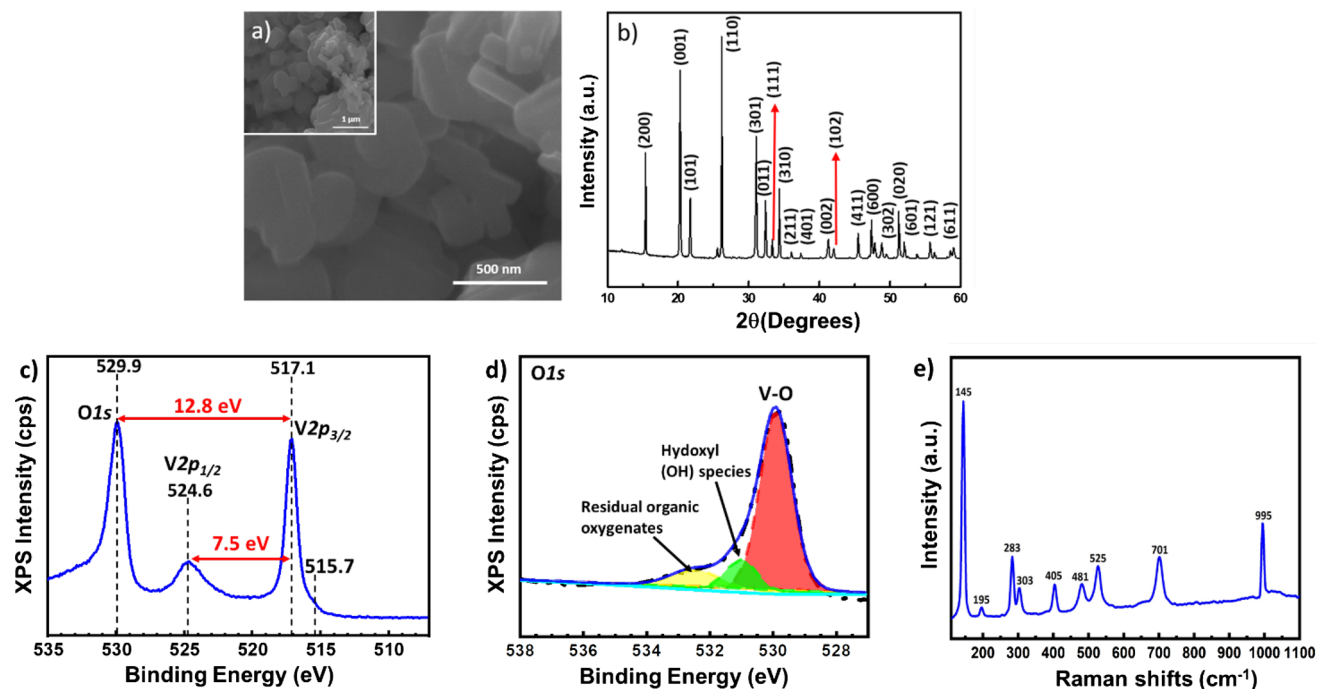


Figure 2 a SEM images of V_2O_5 powder at different magnifications (500 nm and 1 μ m). b XRD pattern of V_2O_5 powder. Regional XPS spectra for c $V2p$ and d $O1s$ core levels of V_2O_5 powder. e Raman spectrum of V_2O_5 powder.

bond [49–51], provided in Fig. 2d. $O1s$ signals at 531.0 and 532.4 eV can be assigned to chemisorbed hydroxyl (OH) species [52, 53] and C=O/C–O(H) [17, 53, 54] residual organic oxygenates on the surface, respectively (Fig. 2d).

Raman spectroscopy was utilized to further characterize the structure of V_2O_5 powder. Figure 2e reveals V_2O_5 powder with Raman features located at around 145, 195, 283, 303, 405, 481, 525, 701, and 995 cm^{-1} . Commercial V_2O_5 powder and thin film peak positions were discovered to be in excellent concurrence with those described in the literature [17, 55–58]. The vanadyl mode associated with the stretching of V–O brought on by unshared oxygen was responsible for the high-frequency Raman peak at 995 cm^{-1} [17, 50, 59]. The structural quality of the V_2O_5 nanoparticles was proved by the presence of this peak. Peaks located at 525 and 701 cm^{-1} were assigned to the stretching vibrations, and those at 303 and 481 cm^{-1} were related to bending vibrations of the V–O–V bridging bonds [17, 60, 61]. Peaks at 283 and 406 cm^{-1} were attributed to V=O bond bending vibration [62, 63]. On the other hand, the lattice vibrations of O–V–O atoms were represented by the Raman peaks at 145 and 197 cm^{-1} in the low-frequency zone [52, 64]. The layered structure of V_2O_5 was directly related to these

two peaks [45]. The peak at about 144 cm^{-1} was a rigid, layer-like mode. When the growth temperature was above 300 $^{\circ}C$, the presence of this peak was indicative of the layer-like structure of V_2O_5 films [65].

Morphological analysis of PVP/ V_2O_5 composite nanofibers

The SEM micrographs shown in Fig. 3 show that uniform and cylindrical nanofibers were produced in each case. Moreover, the diameters of the composite nanofibers were found to be thinner than the unfilled (PVP) ones (Table 1). This trend was also noted in the literature [66], associating the reduction in nanofiber diameter with increased surface charge of the polymer jet. The presence of nanoparticles that are more conductive than the polymer induces strong elongational forces that are applied on the jet, and therefore thinner nanofibers are formed [66–68]. Nevertheless, no definitive conclusions can be drawn regarding the impact-increased nanofiller content, as the average diameters of PVP/ V_2O_5 -8 and PVP/ V_2O_5 -10 nanofibers exhibited a certain degree of similarity. To get better observation of the nanoparticles in PVP nanofibers, higher-resolution images are also provided as insets for composite

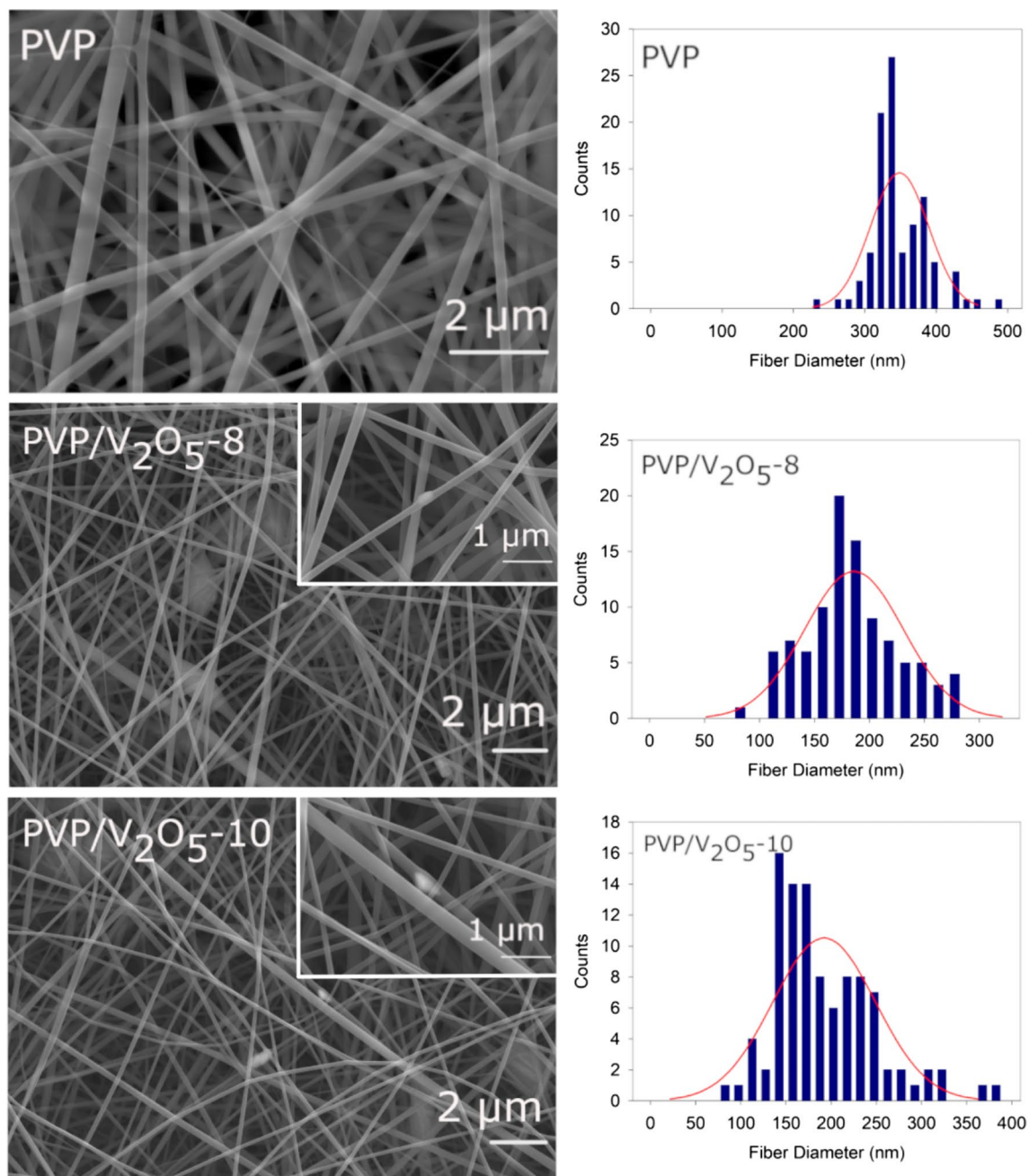


Figure 3 SEM micrographs and diameter distributions of produced PVP/V₂O₅ composite nanofibers. Insets show high-resolution SEM images of nanofibers.

Table 1 Average diameters of the produced nanofibers

Samples	Average diameters (nm)
PVP	349 ± 40.6
PVP/V ₂ O ₅ -8	186 ± 44.8
PVP/V ₂ O ₅ -10	192 ± 56.8

nanofibers. The V₂O₅ nanoparticles were well incorporated into the PVP matrix of the nanofibers as shown in Fig. 3. The nanoparticles were clearly visible in the inset micrographs. These results are also confirmed by EDS maps provided in Fig. 4. As expected, vanadium (V) is particularly localized on the nanoparticles entrapped in the nanofibers.

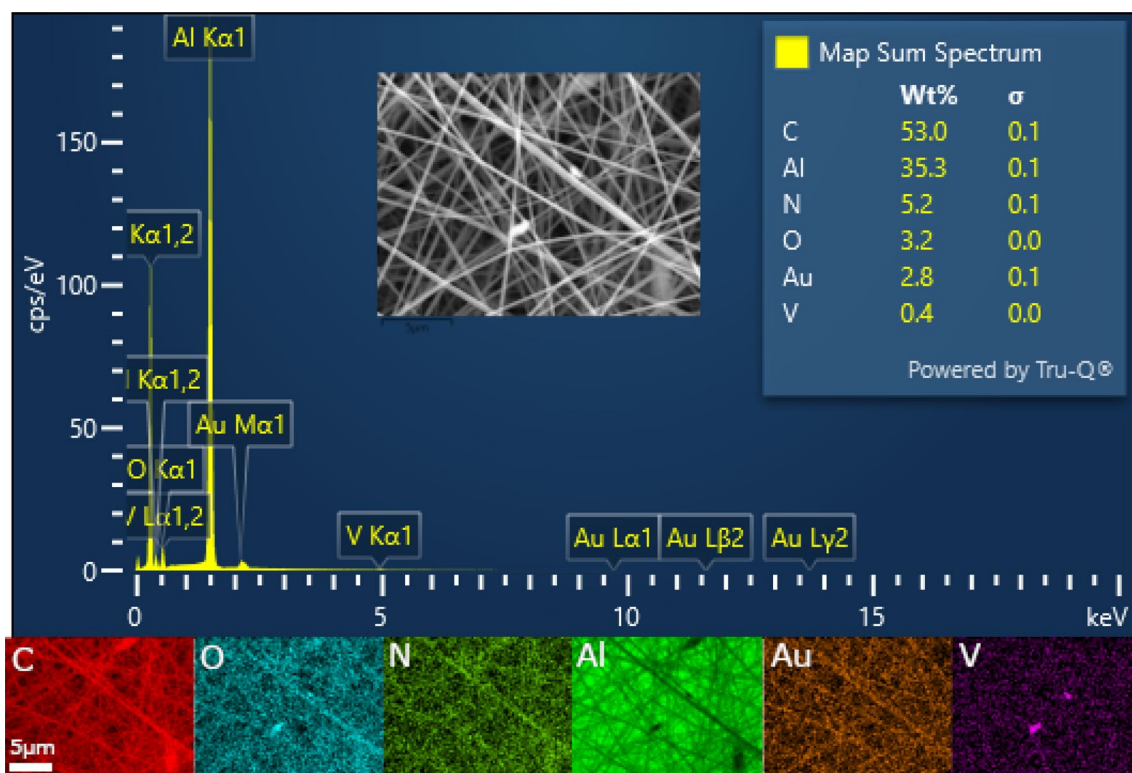


Figure 4 EDS spectrum and corresponding elemental composition and mapping of PVP/V₂O₅ composite nanofibers. The analysis area is given as inset.

The primary elements, carbon (C), oxygen (O), and nitrogen (N), which were the constituents of PVP, were found to be concentrated on the nanofibers. Presence of gold (Au) was due to the sputter coating of the nanofibers. The presence of aluminum (Al) was due to the use of Al tape.

Linear optical analysis of PVP/V₂O₅ composite nanofibers

The linear optical absorption spectra of the composite nanofibers are provided in Fig. 5a. As shown in this figure, two absorption peaks were observed at wavelengths of 400 nm and 217 nm. The observed broad absorption at about 400 nm was attributed to the absorption of V₂O₅ nanoparticles in nanofiber mats. On the other hand, the narrow intense absorption peaks observed at 217 nm were attributed to the PVP matrix. The determined absorption behaviors also indicated that the increasing concentration of V₂O₅ nanoparticles in the composite nanofibers led to a

decrease in absorption behavior, despite having nearly identical thickness.

A crucial parameter that influences the NA behavior of the composite nanofibers was their band gap. Therefore, they were determined by $(ah\nu)^2$ versus $h\nu$ graphs known as Tauc plots [33], presented in Fig. 5b and c. The band gaps were calculated and provided in these figures. Band gap values of 5.11 and 5.33 eV were obtained using the absorption spectra of PVP. These values were highly consistent with those reported in the literature for PVP [69–72]. The small variation between the band gaps of the composite nanofibers can be due to the differences between their thicknesses. Moreover, the band gap values of PVP/V₂O₅-8 and PVP/V₂O₅-10 composite nanofibers were found to be 2.26 and 2.52 eV, respectively. These values were found to be compatible with the literature [73–75]. Urbach energy of the materials was the second important parameter to explain NA mechanisms. By identifying the efficient NA mechanisms, the design of effective optical limiters can be achieved. The expression of

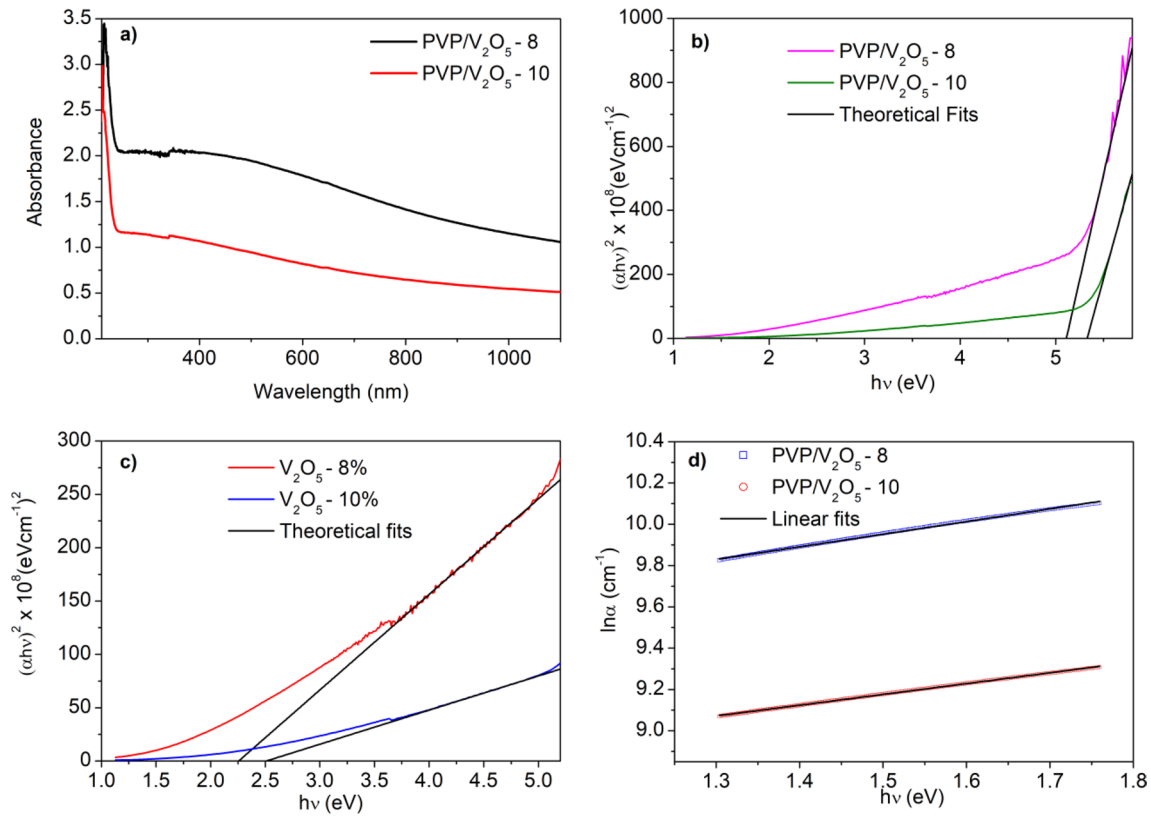


Figure 5 **a** Absorbance spectra and $(\alpha h\nu)^2$ versus $h\nu$ graphs (Tauc plots) of the **b** composite nanofibers and **c** V_2O_5 nanoparticles. **d** $\ln \alpha$ versus $h\nu$ plot of the composite nanofibers.

the Urbach energy of the materials revealed using their linear absorption results is given below.

$$\alpha = \alpha_0 \exp\left(\frac{h\nu}{E_U}\right) \tag{1}$$

where E_U is the Urbach energy, α is the absorption coefficient, and α_0 is a constant. The Urbach energies of the composite nanofibers are determined from inverse slope of the linear region in $\ln \alpha$ versus $h\nu$ graph which is provided in Fig. 5d. The Urbach energies were determined as 1.63 and 1.91 eV for PVP/ V_2O_5 -8 and PVP/ V_2O_5 -10 composite nanofibers, respectively. This result indicated that the increasing concentration of the V_2O_5 nanoparticles in the PVP nanofibers led to an increase in defect states within the band gap of the composite nanofibers. The large Urbach energy reached for the studied composite nanofibers also demonstrated that the defect states were distributed to the deep energy region inside the band gap.

The photoluminescence spectra of the PVP/ V_2O_5 composite nanofibers given in Fig. 6 are obtained under an excitation wavelength of 300 nm. Both PVP/

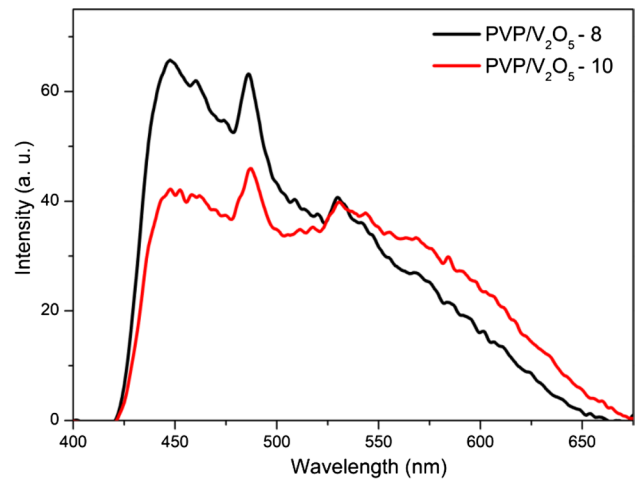


Figure 6 Photoluminescence spectra of the composite nanofibers under 300 nm.

V_2O_5 -8 and PVP/ V_2O_5 -10 composite nanofibers had emission signals at 447, 484, 545, and 568 nm. The energy of the 447- and 484-nm peaks corresponded to

the absorption band edge of the polymer. Therefore, these emission signals occurred during the transition of electrons from the defect states of the polymer to the valence band. On the other hand, the energies of 545 and 568 nm are corresponded to the absorption band edge of the V_2O_5 nanoparticles. Therefore, these emission signals originated during the transition of electrons from defect states to the valence band of the V_2O_5 nanoparticles. Besides, it was seen that the fluorescence intensity of these defect states was reduced with increase in the concentration of V_2O_5 nanoparticles in the polymer.

Nonlinear absorption and optical limiting analysis of PVP/ V_2O_5 composite nanofibers

Nonlinear absorption behaviors of the PVP/ V_2O_5 composite nanofibers were investigated by OA Z-scan measurements at 532 nm with 4-ns pulsed laser. The linear transmittance of the PVP/ V_2O_5 -8 and PVP/ V_2O_5 -10 composite nanofibers was 44% and 61%, respectively. These experiments were performed

at pulse energies of 0.5, 1, and 1.5 μ J. The obtained experimental data with theoretical fits are presented in Fig. 7. It was clearly seen that all of the composite nanofibers presented a NA behavior. As seen in Fig. 7a, the NA increased with an increase in input intensity. On the other hand, the NA decreased with increasing input intensity as can be seen in Fig. 7b. This observation was attributed to filling of the defect states by one-photon absorption (OPA). As reported in the above section, these composite nanofibers have more defect states. Absorption from valence band to these defect states and/or absorption from these defect states to upper excited states would contribute to NA. Therefore, a theoretical fit model [Eq. (2)] considering the contribution of OPA, two-photon absorption (TPA), and free carrier absorption (FCA) to NA was used to determine the NA parameters such as nonlinear absorption coefficient (β_{eff}) and saturable intensity threshold (I_{SAT}) values. These parameters are more important for the optical limiting behavior of the materials. In this model, the first term represents the OPA and its saturation, the second term corresponds

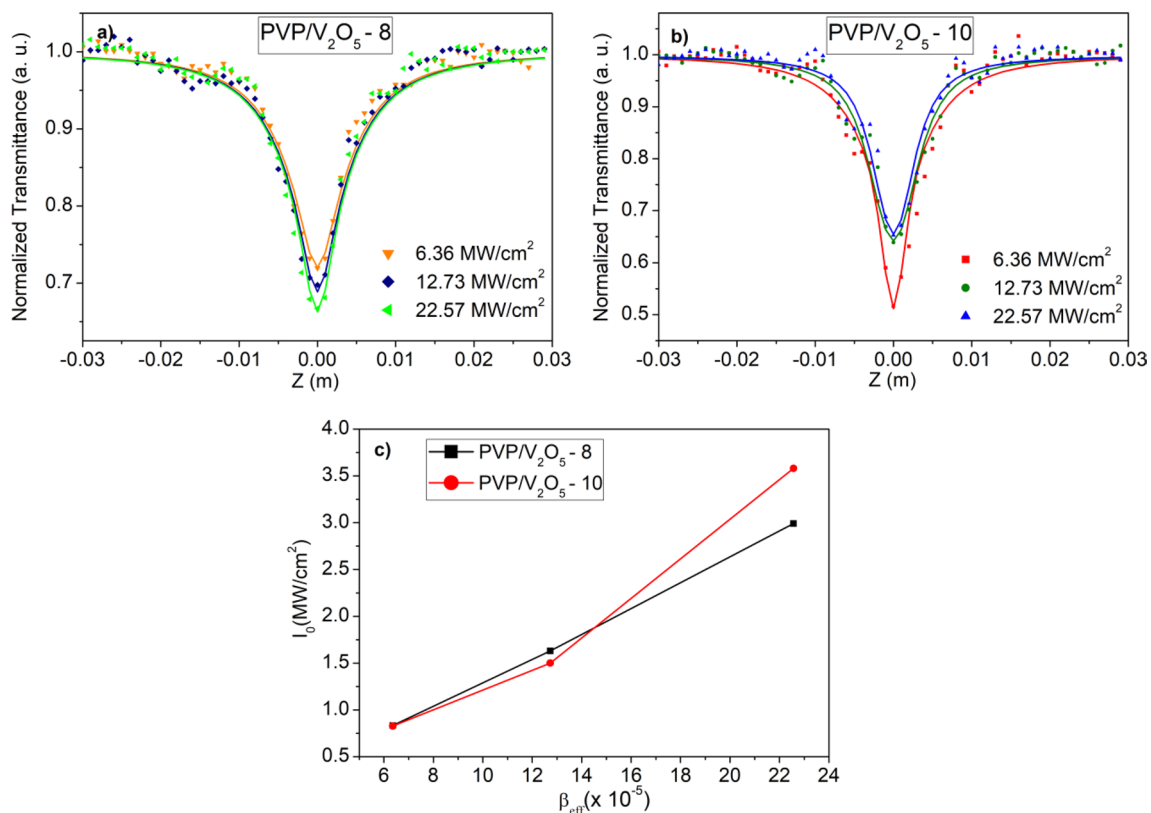


Figure 7 Normalized transmittance of **a** PVP/ V_2O_5 -8 and **b** PVP/ V_2O_5 -10 composite nanofibers at various input intensities, and **c** variation of β_{eff} with respect to input intensities.

to the two-photon absorption (TPA) and its saturation, and the third term deals with free carrier absorption (FCA) and its saturation.

$$\frac{dI}{dz} = \frac{\alpha I}{1 + I/I_{SAT}} - \frac{\beta I^2}{1 + I^2/I_{SAT}^2} - \frac{\sigma_0 \Delta N(I) I}{1 + I^2/I_{SAT}^2} \quad (2)$$

$\Delta N(I)$ is the generated photocarrier density, and β_{eff} is the effective NA coefficient given as

$$\Delta N = \frac{\alpha I}{\hbar\omega} \tau_0 \quad (3)$$

$$\beta_{eff} = \beta + (\sigma_0 \alpha \tau_0 / \hbar\omega) \quad (4)$$

where α is the linear absorption coefficient, $\hbar\omega$ is the photon energy, β is the TPA coefficient, τ_0 is the pulse duration, and σ_0 is the FCA cross section. The following expression can be obtained by substituting Eqs. (3) and (4) in Eq. (2). The beam waist at the focus and Rayleigh length of the composite nanofibers are 25 μm and 0.36 cm, respectively.

$$\frac{dI}{dz'} = -\frac{\alpha I}{1 + I/I_{SAT}} - \frac{\beta_{eff} I^2}{1 + I^2/I_{SAT}^2} \quad (5)$$

Fitting details can be found in the literature [76]. The obtained fitting results are listed in Table 2. The β_{eff} value of the PVP/V₂O₅-8 composite nanofibers increased from 8.32×10^{-6} to 2.99×10^{-5} m/W with an increase in the input intensity. Similarly, the β_{eff} value increased from 8.27×10^{-6} to 3.58×10^{-5} m/W with an increase in the input intensity. As it can be clearly seen in Table 2, the β_{eff} value increased with the V₂O₅ nanofiller amount in the nanofibers. Similarly, I_{SAT} values of both composite nanofibers increased with the input intensity, and the higher value was obtained for the PVP/V₂O₅-10 composite nanofibers. These results could be described with possible NA mechanism

of composite nanofibers. Taking into account the energy band gap values and Urbach energies of V₂O₅ nanoparticles and PVP, the OPA excites an electron from the valence band to the conduction band of V₂O₅ nanoparticles. There is no contribution that comes to NA from the defect states of V₂O₅ nanoparticles for PVP/V₂O₅-8 composite nanofibers. These electrons in the conduction band of V₂O₅ nanoparticles could be excited to the defect states of PVP via excited-state absorption (ESA) considering the energy band gap value of PVP/V₂O₅-8 composite nanofibers, and then, they could be excited to the conduction band of PVP with multiphoton absorption. On the other hand, for PVP/V₂O₅-10 composite nanofibers, the OPA was enough to excite an electron from the valence band to the defect states of V₂O₅ nanoparticles. Some of these electrons could have lost a part of their energy and cooled down to lower excited states, and they could be excited to the defect states of the PVP via ESA. The OPA + ESA process is known as the sequential two-photon absorption (TPA). For this NA mechanism, the β_{eff} value decreases or increases depending on the input intensity. The plot of β_{eff} with respect to input intensity presented in Fig. 7c shows this NA mechanism. A dramatic rise in β_{eff} was observed with increasing input intensity. In PVP/V₂O₅-10 composite nanofibers, an electron in defect states of PVP could be excited to the conduction band of PVP by the absorption of another photon (multiphoton absorption). Considering all of these NA mechanisms, the reason of the obtained stronger NA for PVP/V₂O₅-10 composite nanofibers was the contribution of sequential TPA which was assisted by defect states of V₂O₅ nanoparticles. In our previous report [33], the NA coefficient values of the as-deposited and annealed V₂O₅ thin films were found in the range of 3.85×10^{-7} and 1.02×10^{-6} cm/W. The present composite nanofibers exhibit a 100 times higher NA coefficient values. It is well-known that NA behavior of the materials is very sensitive to production method,

Table 2 The nonlinear absorption coefficients (β_{eff}), saturation intensity threshold (I_{SAT}), and optical limiting threshold values (OLT) of the PVP/V₂O₅ composite nanofibers

I_0 (MW/cm ²)	PVP/V ₂ O ₅ -8			PVP/V ₂ O ₅ -10		
	I_{SAT} ($\times 10^{12}$ W/m ²)	β_{eff} ($\times 10^{-6}$ m/W)	OLT ($\times 10^{-5}$ J/cm ²)	I_{SAT} ($\times 10^{12}$ W/m ²)	β_{eff} ($\times 10^{-6}$ m/W)	OLT ($\times 10^{-5}$ J/cm ²)
6.36	2.79	8.27 ± 0.24		9.78	8.32 ± 0.24	
12.73	10.4	13.3 ± 0.4		19.3	15.0 ± 0.45	
22.57	10.8	29.9 ± 0.89	2.16	38.6	35.8 ± 1.07	1.49

morphology, band gap value, amount and distribution of the defect states, and possible NA mechanisms. In the case of composite nanofibers, the defect levels of PVP also contributed to possible NA mechanisms. Increasing defect levels and thus NA mechanisms induced larger NA behavior in PVP/V₂O₅ composite nanofibers.

In order to reveal TPA coefficient values of the composite nanofibers, the OA Z-scan curves were fitted to TPA procedure introduced by Sheik-Bahae et al. [24]. The TPA coefficient is found from fitting of OA Z-scan data into Eq. (4).

$$T(z) = \sum_{m=0}^{\infty} \frac{q_0}{(m+1)^{3/2} \left(1 + z^2/z_0^2\right)^m} \quad (6)$$

where m is an integer, $q_0(z)$ is $\beta I_0 L_{\text{eff}}$, β is the TPA coefficient, and the effective thickness is $L_{\text{eff}} = \frac{1 - e^{-\alpha_0 L}}{\alpha_0}$ with the sample thickness L , and α_0 is the linear absorption coefficient. Figure 8 indicates the OA Z-scan curves of the composite nanofibers with their theoretical fits at various input intensities. The TPA coefficient values of PVP/V₂O₅-8 composite nanofibers were found as 2.64×10^{-7} , 0.94×10^{-7} , and

0.51×10^{-7} m/W for 6.36, 12.73, and 22.57 MW/cm² input intensities, respectively. Besides, the TPA coefficient values of PVP/V₂O₅-10 composite nanofibers were found as 2.93×10^{-7} , 1.63×10^{-7} , and 1.13×10^{-7} m/W for 6.36, 12.73, and 22.57 MW/cm² input intensities, respectively. These results indicated that the increased V₂O₅ nanofiller in PVP nanofibers caused greater TPA coefficient. As compared the TPA coefficient values with NA coefficient values, it was clear seen that the absorption depends on the defect states that contribute to NA and cause stronger NA behavior in the composite nanofibers. Saravanakannan et al. reported the TPA coefficient value of the V₂O₅ nanoparticles in solution to be 3.19×10^{-10} m/W [32]. This result was smaller than that of our samples' TPA coefficient values. This difference can be attributed to contribution of defects to TPA. The results of similar studies are listed in Table 3. At the same excitation condition, the NA coefficient values of the PVP/V₂O₅ composite nanofibers are higher than that of listed results in Table 3. Considering nanoparticles having high surface-to-volume ratio and nanofibers having high aspect ratio (length to diameter ratio), combined nanoparticles-filled nanofibers led to increased light-matter interaction, which resulted in the

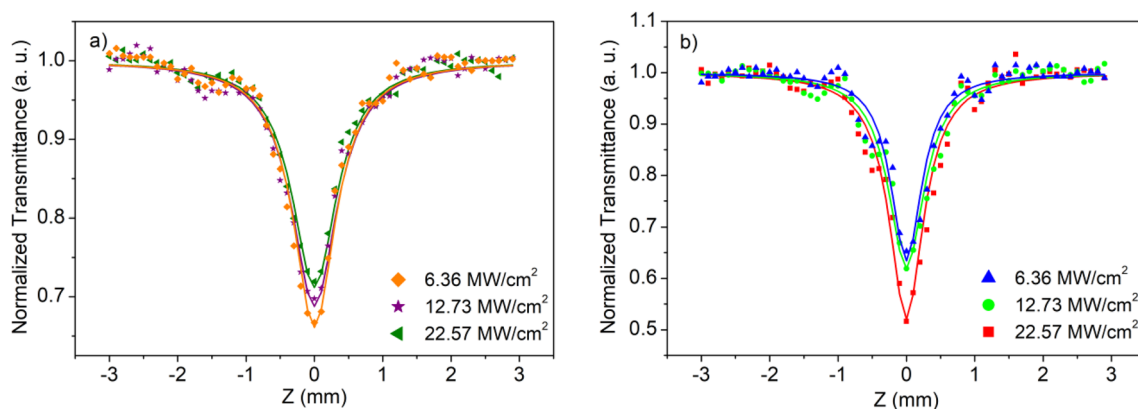


Figure 8 OA Z-scan curves and TPA theoretical fits of PVP/V₂O₅ composite nanofibers at various input intensities.

Table 3 Comparison of NA coefficient and OLT values of reported nonlinear optical materials

Samples	NA coefficient (m/W)	OLT (J/cm ²)	Refs.
Benzil-poly(methyl methacrylate) (PMMA) nanofibers (9 ns, 532 nm)	2.1×10^{-10}	4.59	[33]
Potassium dihydrogen phosphate (KDP)-polyethylene oxide (PEO) nanofibers (5 ns, 532 nm)	3.55×10^{-10}	0.49	[34]
Cd-Fe co-doped CuO nanoparticles in solution (5 ns, 532 nm)	4.80×10^{-10}	1.40	[78]
Thulium-doped barium tellurite glasses (9 ns, 532 nm)	1.35×10^{-10}	2.14	[79]

strengthening of NA. It is clear that these properties will be different for different morphologies, which were strongly affected by the electrospinning process and material parameters such as solution concentration, polymer density, high voltage applied, solvent, and molecular weight of the polymer. George et al. attributed the effective nonlinear absorption and optical limiting threshold to the enhanced light–matter interactions in nanofibrous morphologies [77]. Therefore, this result can be also attributed to a higher light–matter interaction in PVP/V₂O₅ composite nanofibers.

An ideal OL has high transparency in the open state, which allows for IR imaging, and high transparency in the limited state, which prevents damage from high-intensity light [78–81]. Stronger NA, nonlinear scattering, and nonlinear refraction features cause stronger optical limiting features of the materials under high input intensity. The optical limiting curves of the composite nanofibers at 22.57 MW/cm² input intensity are presented in Fig. 9. The obtained values are listed in Table 2. The value of optical limiting threshold (OLT) was obtained to be 2.16×10^{-5} J/cm², and it was found to decrease to 1.49×10^{-5} J/cm² with increasing the content of V₂O₅ nanofillers in polymer. This phenomenon was due to the stronger NA behavior of 10 wt% V₂O₅ nanoparticles-filled nanofibers when compared to 8 wt% V₂O₅ nanoparticles-filled ones. It is clear that the composite nanofiber mats produced in this study showed better optical limiting performance, with a

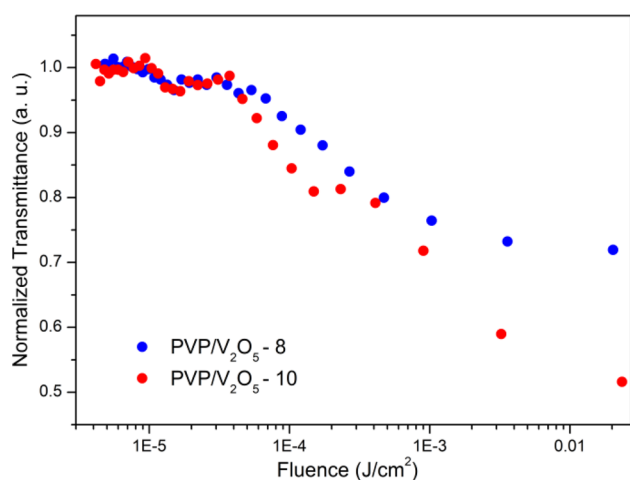


Figure 9 Optical limiting curves of PVP/V₂O₅ composite nanofibers at an input intensity of 22.57 MW/cm².

lowest limiting threshold values at 532 nm compared to benchmark materials [82–84]. To assess the optical limiting performance of the examined nanofibers, a comparison is made with relevant studies in Table 3 from the existing literature. It is observed that the optical limiting behavior of the PVP/V₂O₅ composite nanofibers surpasses that of the studies listed. These findings demonstrated that the V₂O₅ nanofilled PVP composite nanofibers were promising for the fabrication of optical limiters for protecting vulnerable photodetectors and human eyes from hazardous pulsed laser radiation.

Conclusions

In this paper, V₂O₅ nanoparticles synthesized by hydrothermal method were used as nanofillers in electrospun PVP nanofibers. XRD analysis proved the purity of the synthesized V₂O₅ nanopowder. SEM results showed that V₂O₅ nanoparticles were well incorporated into the PVP nanofibers. Linear absorption results revealed two absorption bands at around 400 and 217 nm which were related with the PVP and V₂O₅ nanoparticles, respectively. The results also revealed that the increasing nanofiller content increased the Urbach energy from 1.63 to 1.91 eV in the composite nanofibers. The OA Z-scan experiments were performed at 532 nm to reveal the defect states effect on the NA behavior of the composite nanofibers. It was revealed that the β_{eff} value increased from 2.99×10^{-5} to 3.58×10^{-5} m/W with the increase in V₂O₅ nanoparticle content at the same input intensity. The reason of this observation was ascribed to the possible occurring of NA mechanisms. In PVP/V₂O₅-8 composite nanofibers, the main NA mechanism was the OPA, and there was no contribution of the defect states of V₂O₅ nanoparticles. On the other hand, sequential TPA was the main NA mechanism in PVP/V₂O₅-10 composite nanofibers. In the present composite nanofibers, the defect states of the V₂O₅ nanoparticles, especially, induced the higher NA behavior. The lower optical limiting threshold was obtained for PVP nanofibers with the highest V₂O₅ nanoparticle content as 1.49×10^{-5} J/cm². The combination of high linear transmittance at low input intensity and robust NA behavior at high input intensity renders PVP/V₂O₅-10 composite nanofibers as exceptionally promising candidates for optical limiters in the visible wavelength region.

Author contributions

YP and YT helped in visualization, investigation, data curation, writing—original draft, and writing—review and editing. SA and HEU participated in conceptualization, methodology, resources, and writing—review and editing. NA was involved in resources and investigation. EÇ participated in resources, data curation, and investigation. AK helped in supervision, conceptualization, methodology, and writing—review and editing. AE participated in conceptualization, methodology, and writing—review and editing.

Funding

Open access funding provided by the Scientific and Technological Research Council of Türkiye (TÜBİTAK).

Data availability

The data that support the findings of this study are available upon reasonable request from the authors.

Declarations

Conflict of interest The authors declare that they have no conflict of interest.

Ethical approval Not applicable.

Open Access This article is licensed under a Creative Commons Attribution 4.0 International License, which permits use, sharing, adaptation, distribution and reproduction in any medium or format, as long as you give appropriate credit to the original author(s) and the source, provide a link to the Creative Commons licence, and indicate if changes were made. The images or other third party material in this article are included in the article's Creative Commons licence, unless indicated otherwise in a credit line to the material. If material is not included in the article's Creative Commons licence and your intended use is not permitted by statutory regulation or exceeds the permitted use, you will need to obtain permission

directly from the copyright holder. To view a copy of this licence, visit <http://creativecommons.org/licenses/by/4.0/>.

References

- [1] Izard N, Ménard C, Riehl D, Doris E, Mioskowski C, Anglaret E (2004) Combination of carbon nanotubes and two-photon absorbers for broadband optical limiting. *Chem Phys Lett* 391:124–128
- [2] Wang W, Luo Y, Zhang D, Luo F (2006) Dynamic optical limiting experiments on vanadium dioxide and vanadium pentoxide thin films irradiated by a laser beam. *Appl Opt* 45:3378–3381
- [3] Raja S, Bheeman D, Rajamani R, Bellan C (2016) Structural and optical properties of vacuum evaporated V_2O_5 thin films. *Optik* 127:461–464
- [4] Abbasi M, Rozati S, Irani R, Beke S (2015) Synthesis and gas sensing behavior of nanostructured V_2O_5 thin films prepared by spray pyrolysis. *Mater Sci Semicond Process* 29:132–138
- [5] Panagopoulou M, Vernardou D, Koudoumas E, Katsarakis N, Tsoukalas D, Raptis YS (2017) Tunable properties of Mg-doped V_2O_5 thin films for energy applications: Li-ion batteries and electrochromics. *J Phys Chem C* 121:70–79
- [6] Jerominek H, Picard F, Vincent D (1993) Vanadium oxide films for optical switching and detection. *Opt Eng* 32:2092–2099
- [7] Ureña-Begara F, Crunteanu A, Raskin J-P (2017) Raman and XPS characterization of vanadium oxide thin films with temperature. *Appl Surf Sci* 403:717–727
- [8] Nadkarni G, Shirodkar V (1983) Experiment and theory for switching in Al/ V_2O_5 /Al devices. *Thin Solid Films* 105:115–129
- [9] Moshfegh A, Ignatiev A (1991) Formation and characterization of thin film vanadium oxides: Auger electron spectroscopy, X-ray photoelectron spectroscopy, X-ray diffraction, scanning electron microscopy, and optical reflectance studies. *Thin Solid Films* 198:251–268
- [10] Luo Z, Wu Z, Xu X, Du M, Wang T, Jiang Y (2010) Impact of substrate temperature on the microstructure, electrical and optical properties of sputtered nanoparticle V_2O_5 thin films. *Vacuum* 85:145–150
- [11] Beke S (2011) A review of the growth of V_2O_5 films from 1885 to 2010. *Thin Solid Films* 519:1761–1771
- [12] Liu Y, Jia C, Wan Z, Weng X, Xie J, Deng L (2015) Electrochemical and electrochromic properties of novel

- nanoporous NiO/V₂O₅ hybrid film. *Sol Energy Mater Sol Cells* 132:467–475
- [13] Kim A, Kalita G, Kim JH, Patel R (2021) Recent development in vanadium pentoxide and carbon hybrid active materials for energy storage devices. *Nanomaterials* 11:3213
- [14] Raj AD, Pazhanivel T, Kumar PS, Mangalaraj D, Nataraj D, Ponpandian N (2010) Self assembled V₂O₅ nanorods for gas sensors. *Curr Appl Phys* 10:531–537
- [15] Alrammouz R, Lazerges M, Pironon J, Taher IB, Randi A, Halfaya Y, Gautier S (2021) V₂O₅ gas sensors: a review. *Sens Actuators A* 332:113179
- [16] Yan Z, Shan W, Shi X, He G, Lian Z, Yu Y, Shan Y, Liu J, He H (2020) The way to enhance the thermal stability of V₂O₅-based catalysts for NH₃-SCR. *Catal Today* 355:408–414
- [17] Tutel Y, Durukan MB, Koc S, Koylan S, Cakmak H, Kocak Y, Hekmat F, Ozensoy E, Ozbay E, Udum YA (2021) Multichromic vanadium pentoxide thin films through ultrasonic spray deposition. *J Electrochem Soc* 168:106511
- [18] Zhang Z, Xie W, Li J, Zhang H, Wang Q, Zhang C, Xu G, Gao J, Rogachev A, Cao H (2022) In situ Raman observation of dynamically structural transformation induced by electrochemical lithium intercalation and deintercalation from multi-electrochromic V₂O₅ thin films. *Adv Mater Interfaces* 9:2200883
- [19] Altowyan AS, Hakami J, Algarni H, Shkir M (2023) Enhancing the optoelectronic properties of V₂O₅ thin films through Tb doping for photodetector applications. *J Alloys Compd* 960:170911
- [20] Akl AA (2010) Thermal annealing effect on the crystallization and optical dispersion of sprayed V₂O₅ thin films. *J Phys Chem Solids* 71:223–229
- [21] Raj R, Gupta H, Purohit L (2022) Performance of V₂O₅ hole selective layer in CdS/CdTe heterostructure solar cell. *J Alloy Compd* 907:164408
- [22] Cao W, Zhang J, Lin K, Li J, Dong Y, Xia D, Fan R, Yang Y (2022) Suppressing glass-transition and lithium-ions migration in hole transport layer by V₂O₅ decorated graphite carbon nitride nanosheets for thermally stable perovskite solar cells. *Solar RRL* 6:2200310
- [23] Khadary NH, Almuarqab BT, El Enany G (2023) Nanoparticle-embedded polymers and their applications: a review. *Membranes* 13:537
- [24] Sheik-Bahae M, Said AA, Wei T-H, Hagan DJ, Van Stryland EW (1990) Sensitive measurement of optical nonlinearities using a single beam. *IEEE J Quantum Electron* 26:760–769
- [25] Banfi G, Degiorgio V, Ricard D (1998) Nonlinear optical properties of semiconductor nanocrystals. *Adv Phys* 47:447–510
- [26] Sandeep S, Philip R, Satheeshkumar R, Kumar V (2006) Sol-gel synthesis and nonlinear optical transmission in Zn (1-x) Mg (x) O (x ≤ 0.2) thin films. *Appl Phys Lett* 89:063102
- [27] Banin U, Lee C, Guzelian A, Kadavanich A, Alivisatos A, Jaskolski W, Bryant G, Efros AL, Rosen M (1998) Size-dependent electronic level structure of InAs nanocrystal quantum dots: test of multiband effective mass theory. *J Chem Phys* 109:2306–2309
- [28] Bawendi M, Wilson W, Rothberg L, Carroll P, Jedju TM, Steigerwald M, Brus L (1990) Electronic structure and photoexcited-carrier dynamics in nanometer-size CdSe clusters. *Phys Rev Lett* 65:1623
- [29] Kavan L, Grätzel M, Gilbert S, Klemenč C, Scheel H (1996) Electrochemical and photoelectrochemical investigation of single-crystal anatase. *J Am Chem Soc* 118:6716–6723
- [30] Parida MR, Vijayan C, Rout CS, Sandeep CS, Philip R, Deshmukh P (2011) Room temperature ferromagnetism and optical limiting in V₂O₅ nanoflowers synthesized by a novel method. *J Phys Chem C* 115:112–117
- [31] Poonam D, Mohan S, Bhan K, Yadav M (2022) Barala, Z-scan measurements and optical limiting response of V₂O₅: MoO₃ thin films. *Braz J Phys* 52:194
- [32] Saravanakannan V, Ganesh T, Babeela C, SabariGirisun T, Kalaivani T (2022) A new insight characterization analysis and two photon absorption behaviour of pure and doped vanadium oxide. *Mater Sci Eng, B* 284:115916
- [33] Pepe Y, Tutel Y, Yildiz EA, Karatay A, Unalan HE, Elmali A (2021) Thermally induced phase transition and defect-assisted nonlinear absorption and optical limiting in nanorod morphology V₂O₅ Thin Films. *Adv Eng Mater* 23:2100468
- [34] Anandalli MH, Bhajantri R, Maidur SR, Patil PS (2020) Fluorescence and third-order nonlinear optical properties of thermally stable CBPEA dye-doped PMMA/ZnO nanocomposites. *J Mater Sci: Mater Electron* 31:10531–10547
- [35] Tekin S, Karatay A, Donar YO, Bilge S, Yildiz EA, Snağ A, Elmali A (2021) Tuning the linear and nonlinear optical absorption properties of ZnS/hydrochar nanocomposites by concentration of nanoparticles. *Opt Mater* 113:110849
- [36] Pepe Y, Cevik E, Tutel Y, Karatay A, Unalan HE, Elmali A (2023) Promoting the optical limiting behavior in poly (methyl methacrylate)/α-MnO₂ nanocomposite films through modulation of in-gap states by metal doping. *Mater Chem Phys* 309:128452

- [37] Suresh B, Ramachandran S, Shanmugam G (2023) Effect of Cerium dopant on third-order nonlinear optical properties of CdS/PEG self-standing nanocomposite films. *Opt Mater* 135:113299
- [38] Paul S, Balasubramanian K (2021) Charge transfer induced excitons and nonlinear optical properties of ZnO/PEDOT: PSS nanocomposite films. *Spectrochim Acta Part A Mol Biomol Spectrosc* 245:118901
- [39] Heidari B, Salmani S, Sasani Ghamsari M, Ahmadi M, Majles-Ara MH (2020) Ag/PVP nanocomposite thin film with giant optical nonlinearity. *Opt Quantum Electron* 52:1–18
- [40] Pramod A, Yogeswari C, Singh AK, Girisun TS, Manattayil JK, Raghunathan V, Nagalakshmi R (2024) Nonlinear optical characterisation of electrospun Benzil-PMMA nanofibers. *Opt Laser Technol* 168:109898
- [41] Yogeswari C, Sabari Girisun T, Nagalakshmi R (2021) Excited-state absorption assisted optical limiting action of potassium dihydrogen phosphate (KDP)–polyethylene oxide (PEO) electrospun nanofibers. *J Electron Mater* 50:4619–4632
- [42] Mu J, Wang J, Hao J, Cao P, Zhao S, Zeng W, Miao B, Xu S (2015) Hydrothermal synthesis and electrochemical properties of V_2O_5 nanomaterials with different dimensions. *Ceram Int* 41:12626–12632
- [43] Zhang Y (2017) Synthesis and characterization of hollow VO microspheres for supercapacitor electrode with pseudocapacitance. *Mater Sci-Pol* 35:188–196
- [44] Cao P, Gui X, Navale ST, Han S, Xu W, Fang M, Liu X, Zeng Y, Liu W, Zhu D (2020) Design of flower-like V_2O_5 hierarchical nanostructures by hydrothermal strategy for the selective and sensitive detection of xylene. *J Alloy Compd* 815:152378
- [45] Sun X, Gao R, Wu Y, Zhang X, Cheng X, Gao S, Xu Y, Huo L (2023) Novel in-situ deposited V_2O_5 nanorods array film sensor with enhanced gas sensing performance to *n*-butylamine. *Chem Eng J* 459:141505
- [46] Silversmit G, Depla D, Poelman H, Marin GB, De Gryse R (2004) Determination of the V_{2p} XPS binding energies for different vanadium oxidation states (V^{5+} to V^{0+}). *J Electron Spectrosc Relat Phenom* 135:167–175
- [47] Pei G, Xiang J, Zhong D, Li G, Lv X (2021) Isothermal reduction of V_2O_5 powder using H_2 as oxygen carrier: thermodynamic evaluation, reaction sequence, and kinetic analysis. *Powder Technol* 378:785–794
- [48] Jain A, Manippady SR, Tang R, Nishihara H, Sobczak K, Matejka V, Michalska M (2022) Vanadium oxide nanorods as an electrode material for solid state supercapacitor. *Sci Rep* 12:21024
- [49] Williamson G, Smallman R III (1956) Dislocation densities in some annealed and cold-worked metals from measurements on the X-ray debye-scherrer spectrum. *Phil Mag* 1:34–46
- [50] Baddour-Hadjean R, Pereira-Ramos J, Navone C, Smirnov M (2008) Raman microspectrometry study of electrochemical lithium intercalation into sputtered crystalline V_2O_5 thin films. *Chem Mater* 20:1916–1923
- [51] Strunk J, Bañares MA, Wachs IE (2017) Vibrational spectroscopy of oxide overlayers. *Top Catal* 60:1577–1617
- [52] Mounasamy V, Mani GK, Ponnusamy D, Tsuchiya K, Reshma P, Prasad AK, Madanagurusamy S (2020) Investigation on CH_4 sensing characteristics of hierarchical V_2O_5 nanoflowers operated at relatively low temperature using chemiresistive approach. *Anal Chim Acta* 1106:148–160
- [53] Nguyen HTT, Jung D, Park C-Y, Kang DJ (2015) Synthesis of single-crystalline sodium vanadate nanowires based on chemical solution deposition method. *Mater Chem Phys* 165:19–24
- [54] Lazauskas A, Marcinauskas L, Andrulevicius M (2020) Modification of graphene oxide/ $V_2O_5 \cdot n H_2O$ nanocomposite films via direct laser irradiation. *ACS Appl Mater Interfaces* 12:18877–18884
- [55] Vernardou D, Spanakis E, Katsarakis N, Koudoumas E (2014) Electrodeposition of V_2O_5 using ammonium metavanadate at room room temperature. *Adv Matter Lett* 5:569–572
- [56] Vernardou D, Paterakis P, Drosos H, Spanakis E, Povey I, Pemble M, Koudoumas E, Katsarakis N (2011) A study of the electrochemical performance of vanadium oxide thin films grown by atmospheric pressure chemical vapour deposition. *Sol Energy Mater Sol Cells* 95:2842–2847
- [57] Ramana C, Hussain O, Naidu BS, Reddy P (1997) Spectroscopic characterization of electron-beam evaporated V_2O_5 thin films. *Thin Solid Films* 305:219–226
- [58] Lee S-H, Cheong HM, Seong MJ, Liu P, Tracy CE, Mascarenhas A, Pitts JR, Deb SK (2003) Raman spectroscopic studies of amorphous vanadium oxide thin films. *Solid State Ionics* 165:111–116
- [59] George A, Yang Q (2023) Gas sensing performance of Tungsten doped V_2O_5 nanorod thin-films deposited by hot filament CVD combined with DC sputtering. *Sens Actuators B Chem* 394:134371
- [60] Abd-Alghafour N, Ahmed NM, Hassan Z, Almessiere MA (2018) Hydrothermal synthesis and structural properties of V_2O_5 nanoflowers at low temperatures. *J Phys Conf Ser IOP Pub* 1083:012036

- [61] Sabna M, Jayaram P (2023) Reformed dielectric features in single phase orthorhombic nickel vanadate complex oxides and the significance of the lattice dynamics in the optoelectrical features. *J Phys Chem Solids* 180:111428
- [62] Basu R, Prasad AK, Dhara S, Das A (2016) Role of vanadyl oxygen in understanding metallic behavior of V_2O_5 (001) nanorods. *J Phys Chem C* 120:26539–26543
- [63] Julien C, Nazri G, Bergström O (1997) Raman scattering studies of microcrystalline V_6O_{13} . *Phys Status Solidi B* 201:319–326
- [64] Wachs IE, Jehng J-M, Hardcastle FD (1989) The interaction of V_2O_5 and Nb_2O_5 with oxide surfaces. *Solid State Ionics* 32:904–910
- [65] Beattie I, Gilson T (1969) Oxide phonon spectra. *J Chem Soc A Inorg Phys Theor*. <https://doi.org/10.1039/J19690002322>
- [66] Huang S, Zhou L, Li M-C, Wu Q, Kojima Y, Zhou D (2016) Preparation and properties of electrospun poly (vinyl pyrrolidone)/cellulose nanocrystal/silver nanoparticle composite fibers. *Materials* 9:523
- [67] Pepe Y, Akkoyun S, Bozkurt B, Karatay A, Ates A, Elmali A (2023) Investigation of the wavelength dependent nonlinear absorption mechanisms of polyvinylpyrrolidone and cadmium selenide hybrid nanofibers. *Opt Laser Technol* 164:109497
- [68] Akkoyun Ş (2021) Electrospun polyvinylpyrrolidone/graphite composite nanofiber mats: effect of the filler on the morphology and wettability. *Niğde Ömer Halisdemir Üniversitesi Mühendislik Bilimleri Dergisi* 10:840–846
- [69] Mergen ÖB, Arda E, Kara S, Pekcan Ö (2019) Effects of GNP addition on optical properties and band gap energies of PMMA films. *Polym Compos* 40:1862–1869
- [70] Hussien MS, Mohammed M, Yahia I (2020) Multifunctional applications of graphene-doped PMMA nanocomposite membranes for environmental photocatalytic. *J Inorg Organomet Polym Mater* 30:2708–2719
- [71] Al-Ammar K, Hashim A, Husaen M (2013) Synthesis and study of optical properties of (PMMA-CrCl₂) composites. *Chem Mater Eng* 1:85–87
- [72] Arif S, Saleemi F, Rafique MS, Naab F, Toader O, Mahmood A, Aziz U (2016) Effect of silver ion-induced disorder on morphological, chemical and optical properties of poly (methyl methacrylate). *Nucl Instrum Methods Phys Res Sect B* 387:86–95
- [73] Schneider K (2020) Optical properties and electronic structure of V_2O_5 , V_2O_3 and VO_2 . *J Mater Sci Mater Electron* 31:10478–10488
- [74] Chan Y-L, Pung S-Y, Sreekantan S (2014) Synthesis of V_2O_5 nanoflakes on PET fiber as visible-light-driven photocatalysts for degradation of RhB dye. *J Catal* 2014:370696
- [75] Mrigal A, Addou M, El Jouad M, Khannyra S (2017) Electrochemical performance of the V_2O_5 and VO_2 thin films synthesized by spray pyrolysis technique. *J Mater Environ Sci* 8:3598–3607
- [76] Yüksek M, Kürüm U, Yaglioglu HG, Elmali A, Ateş A (2010) Nonlinear and saturable absorption characteristics of amorphous InSe thin films. *J Appl Phys* 107:033115
- [77] Li H, Chen X, Lu W, Wang J, Xu Y, Guo Y (2021) Application of electrospinning in antibacterial field. *Nanomaterials* 11:1822
- [78] Gadhwal R, Kaushik P, Devi A (2023) A review on 1D photonic crystal based reflective optical limiters. *Crit Rev Solid State Mater Sci* 48:93–111
- [79] Shi Y, Sang P, Yin G, Gao R, Liang X, Brzozowski R, Odom T, Eswara P, Zheng Y, Li X (2020) Aggregation-induced emissive and circularly polarized homogeneous sulfono- γ -AApeptide foldamers. *Advanced optical materials* 8:1902122
- [80] Bugaychuk S, Iljin A, Telbiz G, Zhulai D, Leonenko E, Romanovska N, Gridyakina A, Bordyuh A, Kravchuk M, Polishchuk A (2018) Nonlinear all-optical light valves fabricated on mesoscopic Ti-, Si-substrates. *J Mol Liq* 267:34–37
- [81] Zhang Y, Sui N, Kang Z, Meng X, Yuan L, Li X, Zhang H-Z, Zhang J, Wang Y (2022) Scanning the optoelectronic properties of $Cs_4Cu_xAg_{2-2x}Sb_2Cl_{12}$ double perovskite nanocrystals: the role of Cu^{2+} content. *J Mater Chem C* 10:5526–5533
- [82] Zhu S, Zhang Q, Pan Q, Hu J, Liu R, Song G, Zhu H (2022) High performance Pt (II) complex and its hybridized carbon quantum dots: synthesis and the synergistic enhanced optical limiting property. *Appl Surf Sci* 584:152567
- [83] Chen Y, Bai T, Dong N, Fan F, Zhang S, Zhuang X, Sun J, Zhang B, Zhang X, Wang J (2016) Graphene and its derivatives for laser protection. *Prog Mater Sci* 84:118–157
- [84] Loh KP, Zhang H, Chen WZ, Ji W (2006) Templated deposition of MoS_2 nanotubules using single source precursor and studies of their optical limiting properties. *J Phys Chem B* 110:1235–1239

Publisher's Note Springer Nature remains neutral with regard to jurisdictional claims in published maps and institutional affiliations.